Quantum oscillations in $EuFe_2As_2$ single crystals

P. F. S. Rosa,[1,2] B. Zeng,[3] C. Adriano,[1] T. M. Garitezi,[1] T. Grant,[2] Z. Fisk,[2] L. Balicas,[3] M. D. Johannes,[4] R. R. Urbano,[1] and P. G. Pagliuso[1]

[1]*Instituto de Física "Gleb Wataghin", UNICAMP, Campinas-SP, 13083-859, Brazil*

[2]*University of California, Irvine, California 92697-4574, USA*

[3]*National High Magnetic Field Laboratory, Florida State University, Tallahassee, Florida 32310, USA*

[4]*Center for Computational Materials Science, Code 6390, Naval Research Laboratory, Washington, District of Columbia 20375, USA*

(Received 6 March 2014; revised manuscript received 11 November 2014; published 24 November 2014)

Quantum oscillation measurements provide relevant information about the Fermi surface (FS) properties of strongly correlated metals. Here, we report on the Shubnikov–de Haas effect via high-field resistivity measurements of $EuFe_2As_2$ (Eu122) and $BaFe_2As_2$ (Ba122) single crystals. Although both pnictide compounds are isovalent with similar effective masses and density of states, at the Fermi level, our results reveal subtle changes in their fermiology. Remarkably, although the spin-density-wave (SDW) ordering temperature is higher in the Eu-rich end, Eu122 displays a much more isotropic and three-dimensional-like FS when compared with Ba122, in agreement with band structure calculations. Our experimental results suggest an anisotropic contribution of the Fe $3d$ orbitals to the FS in Ba122. We speculate that this orbital differentiation may be responsible for the suppression of the SDW phase in the FeAs-based compounds.

DOI: 10.1103/PhysRevB.90.195146 PACS number(s): 74.70.Xa, 71.18.+y

I. INTRODUCTION

The Fe-based superconductors (SC) have been a subject of intensive investigation owing to their high superconducting transition temperature T_c reaching values up to 56 K [1–4]. Although all members present FeAs layers as the common structural parameter, there is a variety of dissimilarities in their physical properties, such as magnetic ordered moments, effective masses, size of SC gaps, and T_c itself [5]. For instance, KFe_2As_2 is a nonmagnetic metal which superconducts below 4 K while $BaFe_2As_2$ (Ba122) undergoes a transition from a paramagnetic to a spin-density-wave (SDW) metallic state at 139 K, closely related to a structural transition [6]. Nonetheless, superconductivity can be induced in Ba122 by either hydrostatic pressure and/or chemical substitution (e.g., K, Co, Ni, Cu, and Ru). A deep understanding of such differences still remains an open question. In this regard, it is vital to unveil the Fermi surface (FS) geometry and symmetry, as well as the role of local distortions, given that they might be strongly related to the nature of the magnetic fluctuations in momentum space.

Experimentally, the most widely employed technique to directly access the electronic structure of crystals is angle resolved photoemission spectroscopy (ARPES). For the parent compounds AFe_2As_2 (A = Ba, Ca, Eu, Sr, ...), ARPES data usually display four Fe $3d$ FS sheets in the paramagnetic regime: two electronlike bands around the M point and two holelike bands around the Γ point of the Brillouin zone (BZ). Furthermore, polarized ARPES measurements show the predominance of t_{2g} orbitals (xy, xz/yz) at the FS with the outer hole-pocket being mostly xy, in agreement with density functional theory (DFT) combined with dynamical mean field theory (DMFT) calculations [7–10]. Interestingly, a comparison between Ba122 and $EuFe_2As_2$ (Eu122) in the paramagnetic state reveals that the outer hole xy pocket in Ba122 is half the size of Eu122 [11], suggesting an increase of the planar xy occupation in the Ba-rich end. It is noteworthy that it is possible to change the occupation between distinct t_{2g}, or even e_g, orbitals although the total Fe occupation remains the same. Although such symmetry changes are carried to the FS, their precise influence is not fully understood yet. In addition, as the temperature is lowered below T_{SDW}, further striking consequences, such as FS reconstruction, band splitting, opening of gaps, etc., are expected. Nonetheless, ARPES is a surface sensitive technique and it is highly desirable to confront its results with bulk FS experiments since the electronic structure on the surface may differ from the one in the bulk.

Within this context, the determination of a precise FS by a bulk-sensitive experimental technique is crucial and quantum oscillation (QO) measurements have been proven to be an important complementary technique to ARPES [12,13]. In particular, low temperature QO experiments have been reported on several members of the 122 family AFe_2As_2 (A = Ba, Ca, Sr) providing both high resolution of the FS in momentum space and important information on the effective masses [14–17]. In particular, three low frequency (F) Fourier peaks have been observed for $BaFe_2As_2$ at $F_\delta = 500$, $F_\alpha = 440$, and $F_\gamma = 90$ T, corresponding to the δ (electron), α (hole), and γ (electron) pockets, respectively, each of them occupying about 2% of the nonmagnetic BZ. For Eu122, single crystals with a residual resistivity ratio (RRR) as high as 15 have been synthesized [18]. The semimetal $EuFe_2As_2$ compound is unique because it displays both a SDW phase transition at 190 K and an antiferromagnetic (AFM) phase transition at $T_N = 19$ K due to the Eu^{2+} moments [19]. Interestingly, Eu122 also undergoes a metamagnetic transition at $H_m \sim 2$ T from an AFM state to a ferromagnetic (FM) one [20]. Thus, there is no additional reconstruction of the FS due to the long range ordering of the Eu moments at low temperatures.

In this paper, we report a comparative Shubnikov–de Haas (SdH) study between Eu122 and Ba122 single crystals grown by In flux. Our results for Ba122 are in good agreement with previous reports [14–16] and our observation of QO in Eu122 indicates that the Indium flux technique yields high quality single crystals. Subtle changes in the fermiology of Eu122,

such as band splitting and a significant increase of isotropy and three-dimensionality of the bands, are clearly noticed when comparing the data with those of Ba122. Our main findings shed light on the understanding of the SDW state and provide a possible scenario for the differences in the physical properties of this class of materials.

II. EXPERIMENTAL DETAILS AND THEORETICAL METHODS

Single-crystalline samples of $EuFe_2As_2$ were grown using the Indium flux technique with starting composition Eu:Fe:As:In = 1:2:2:25. The mixture was placed in an alumina crucible and sealed in a quartz tube under vacuum. The sealed tube was heated up to 1100°C for 8 h and then cooled down to 1000°C at 2°C/h. The furnace was then turned off and the excess of In flux was removed at 400°C by centrifugation. Single-crystalline samples of $BaFe_2As_2$ were grown as described in Ref. [21]. Our crystals were checked by X-ray powder diffraction and elemental analysis using a commercial energy dispersive spectroscopy (EDS) microprobe. Specific-heat measurements were performed in a commercial small-mass calorimeter that employs a quasiadiabatic thermal relaxation technique. The in-plane resistivity $\rho_{ab}(T)$ was measured using a standard four-probe method inside a ^{3}He cryostat. Magnetic fields up to 35 and 45 T were applied at the National High Magnetic Field Laboratory in Tallahassee, FL. The samples were discretely rotated between 0° and 90° with an in-plane rotation axis. Here, 0° stands for H parallel to the c axis.

The theoretical Fermi surfaces were calculated using density functional theory with a full-potential augmented plane wave code, Wien2k [22], using the local density approximation (LDA) [23] and its extension, LDA+U [24] to remove the localized Eu f states from the Fermi level E_F. The presented calculations employ a "U"value of 8 eV and a "J"value of 1 eV, where U is the effective on-site Coulomb interaction and J is the effective on-site exchange between electrons on a single Eu ion. Nevertheless, the electronic structure within several eV of E_F is insensitive to this particular choice. The experimental lattice parameters and atomic positions were extracted from Refs. [25] and [26] for the Eu and Ba based systems, respectively. We established the so-called magnetic "stripe"phase in which the basic unit cell is doubled both in-plane and along the c axis to account for the antiferromagnetic ordering in both directions, resulting in an orthorhombic cell (space group 53). For the Eu compound, the Eu moments are aligned with each other in-plane and between planes, in agreement with the experimentally observed ferromagnetic state at high fields [27]. We used a mesh of 23 × 23 × 7 points in the irreducible Brillouin zone.

III. RESULTS AND DISCUSSION

Figure 1 displays $\rho_{ab}(T)$ at zero magnetic field for the studied compounds. A linear metallic behavior is observed down to T_{SDW} where a sudden drop is identified in the curves of Eu122 and Ba122 at 193 and 139 K, respectively. The transition to a SDW state can also be seen as a sharp peak in the specific heat of both compounds (right hand side inset of Fig. 1). In addition, as the temperature is further decreased, a second drop is observed in Eu122 due to the Eu^{2+} AFM ordering at 19 K (left hand side inset to Fig. 1). Residual resistivity and RRR values for Eu122 are $\rho_0 \simeq 10\ \mu\Omega$ cm and RRR $\simeq 25$, respectively, indicating a high degree of crystallinity.

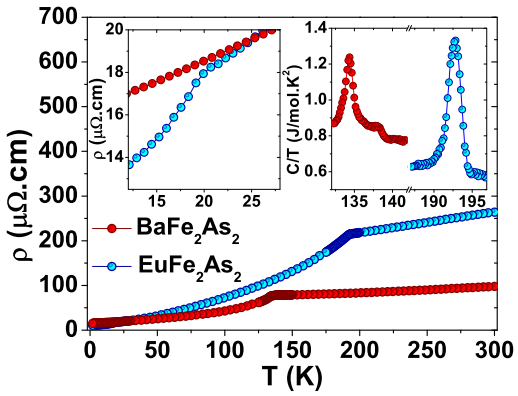

FIG. 1. (Color online) Zero field in-plane resistivity ρ_{ab}(T) for Eu122 and Ba122 single crystals. The left hand side inset shows the Eu^{2+} AFM ordering temperature and the right hand side inset shows the SDW anomaly in the specific heat for both samples.

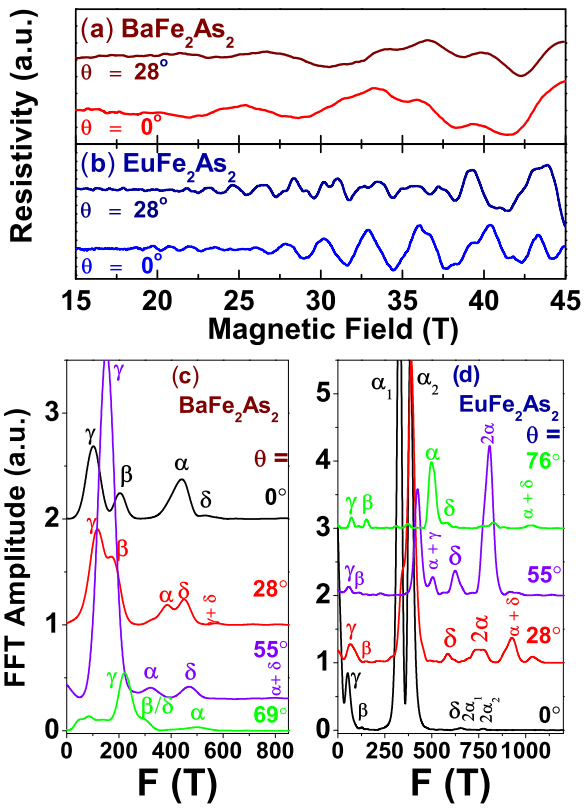

FIG. 2. (Color online) $\rho_{ab}(T)$ as a function of the magnetic field for (a) $EuFe_2As_2$ and (b) $BaFe_2As_2$ single crystals at 0° and 25°, after subtracting a 4th order polynomial background. Here, 0° stands for H parallel to the c axis. (c) and (d) are the FFT amplitudes of the QO of the data in (a) and (b), respectively.

TABLE I. Comparison between the SdH parameters of Ba122 and Eu122 obtained experimentally and theoretically in this work. Negative effective masses mean hole pockets.

	$BaFe_2As_2$						$EuFe_2As_2$					
Pocket	$F(T)$	A/A_{BZ} (%)	m^*/m_e^*	$m^*_{\rm DFT}/m_e^*$	R	T_D (K)	$F(T)$	A/A_{BZ}	m^*/m_e^*	$m^*_{\rm DFT}/m_e^*$	R	T_D
γ	90(10)	0.3	0.7(2)	0.4	2.1	5(2)	60(10)	0.2	1.0(2)	0.4	1.2	
α	430(10)	1.4	1.5(2)	−0.8	2.1	4(1)	340(10)/380(10)	1.3	1.5(2)/1.9(2)	−0.8	1.4	4(1)
δ	510(10)	1.7		1.2	0.8	3(1)	580(10)	1.4		1.7	0.5	3(1)

Figures 2(a) and 2(b) show $\rho_{ab}(T)$ at 0.3 K of our Eu122 and Ba122 single crystals as a function of applied magnetic field, respectively. After subtracting a smooth 4th order polynomial background, anisotropic QO are clearly observed above ∼15 T. The fast Fourier transform (FFT) of these QO as a function of frequency is presented in Figs. 2(c) and 2(d). Four distinct low frequency peaks can be identified for both compounds. The corresponding frequencies are listed in Table I by adopting an identical labeling of the branches as in Ref. [16]. In particular, as of Ref. [15], we also attribute the frequency β to the second harmonic of the γ orbit due to their similar angular dependency in both compounds. It is worth noting that, except for F_δ, all other pockets are slightly smaller in Eu122, suggesting a subtle change of fermiology.

Remarkably, Eu122 presents a band splitting in the predominant α pocket, in agreement with ARPES measurements below $T_{\rm SDW}$ [7]. In addition, combinations of smaller orbits are observed at higher frequencies for both compounds, as reported previously in Ba122 [28], although we were able to identify such frequencies more clearly in Eu122, likely due to its higher signal-to-noise ratio. In the present study, the combination of frequencies can be ascribed to two main reasons. First, magnetic interactions between carriers may give rise to nonlinear coupling of Fermi surface orbits and, ultimately, frequency mixing. In fact, the formation of the spin-density wave phase at low temperatures corroborates with this scenario. Nevertheless, the combination of orbits may be also due to magnetic field-induced tunneling from one part of the FS to another, i.e., magnetic-breakdown orbits. An estimate of the breakdown field gives $B \sim m^* E_g/\hbar e E_F \sim$ 18 T, which is within our experimental range. Here, B is the breakdown field, $E_g \sim 190$ K ~ 16 meV is the gap energy, $E_F \sim 120$ meV is the Fermi energy extracted from the band structure calculations in Ref. [15], and m^* is the effective mass extracted from our experiments. However, we emphasize that such estimate assumes a separation between orbits in k space of the order of this gap.

We now investigate how the observed frequencies evolve with temperature. FFT signal amplitudes with increasing temperature are shown in Fig. 3(a) for Eu122. The corresponding suppression of the SdH signal amplitude as a function of temperature is shown in Figs. 3(b) and 3(c) for Eu122 and Ba122, respectively. Such suppression allows one to extract the corresponding effective masses by fitting the FFT amplitude divided by temperature (A/T) with the thermal damping term $R_T = X/\sinh(X)$ of the Lifshitz-Kosevick (LK) formalism [solid lines in Figs. 3(b) and 3(c)], where $X = 14.69 m^* T/B$ and m^* is the effective mass and $1/B$ is the average inverse field of the Fourier window. Our analysis was not able to determine with accuracy the effective masses for δ and β pockets in Ba122. Concerning the δ pocket, the amplitude determination with increasing temperature is hindered by the lower signal-to-noise ratio due to a very weak FFT signal amplitude, as observed previously in Ref. [15]. In the β pocket, the slight variation of position with temperature yields an inaccurate effective mass determination. Our results for the effective masses of Ba122 and Eu122 are shown in Table I and a comparison to the results obtained previously for Ba122 is presented in Table II. Such comparison reveals that m^* is similar in Ba122 and Eu122 compounds, indicating roughly the same degree of correlation in both compounds. In addition, the estimated Dingle temperature $T_{\rm D}$ is roughly the same for all pockets of both compounds. Therefore, we infer that there must be another prevailing cause for the higher T_{SDW} in Eu122.

In order to unveil this matter, we now turn our attention to the angle dependence of the extremal orbits in Eu122 and Ba122 compounds, shown in Fig. 4. Interestingly, the anisotropy of the pockets displays the most contrasting

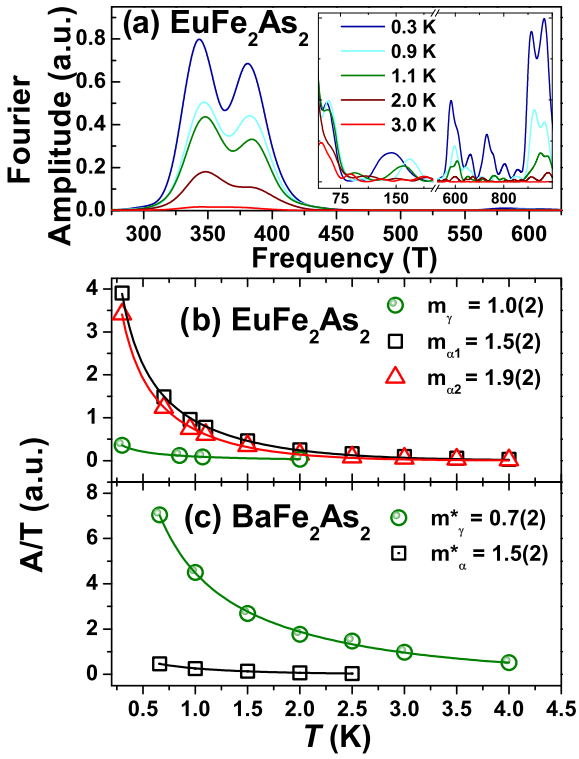

FIG. 3. (Color online) (a) FFT amplitude of the Eu122 compound as a function of frequency for several temperatures. The inset displays less intense peaks. The FFT amplitude divided by temperature A/T as a function of temperature for (b) the observed pockets of Eu122 and (c) the observed pockets of Ba122.

TABLE II. Comparison between the SdH frequencies of Ba122 obtained experimentally in Refs. [15,16]

	$BaFe_2As_2$ (Ref. [15])				$BaFe_2As_2$ (Ref. [16])			
Pocket	$F(T)$	A/A_{BZ} (%)	m^*/m_e^*	T_D (K)	$F(T)$	A/A_{BZ}	m^*/m_e^*	T_D
γ	80(10)	0.3	0.7(2)	3(1)	∼90		0.9(1)	
α	440(10)	1.7	1.2(3)	4(1)	∼440	1.3	2.1(1)	4(1)
δ					∼500	1.4	2.4(3)	3(1)

behavior of our study. On one hand, Fig. 4(b) shows an anisotropic behavior for γ, β ($=\gamma$), and δ pockets in Ba122. The highly eccentric branches γ and β are associated with large quasi-two-dimensional (2D) cylinders which show the expected $1/\cos(\theta)$ dependence (solid lines) and ellipsity of ∼5. On the other hand, Fig. 4(a) presents fairly isotropic branches for the γ and δ pockets in Eu122. Such isotropy extends over the entire angular range and suggests the presence of largely three-dimensional isotropic FS sections. In addition, the α (hole) pocket for both compounds displays a weaker angular dependence that cannot be fitted to $1/\cos(\theta)$, suggesting that this particular isotropic pocket remains unaltered in the series.

All the above experimental results allow us to conclude that the FS sheets in Ba122 are much more 2D than in Eu122, suggesting that the bidimensional/planar (xy and/or x^2-y^2) orbital contribution to the Fe $3d$ bands is higher in $BaFe_2As_2$. In fact, our result is in complete agreement with ARPES measurements in Ba122 and Eu122, which revealed that the hole xy pocket in Ba122 is half the size of Eu122 due to an increase of the planar xy occupation in the Ba-rich end [11]. Interestingly, one might expect that the lower dimensionality of Ba122 would favor a higher T_{SDW}, as compared with Eu122. However, the opposite behavior is found experimentally here, and T_{SDW} is about 50 K lower in Ba122. As the SDW state in these materials is believed to be associated with itinerant Fe $3d$ bands, it is plausible that an increase in the planar character of the bands could destabilize the three-dimensional (3D) itinerant SDW state.

Although we believe that the interpretation of the experimental results is quite consistent, it is desirable to confront the reported data with band structure calculations, when available. Rigorous band structure calculations for $EuFe_2As_2$ are not an easy task due to the presence of the Eu $4f$ electrons. However, we will show that a fairly good agreement with the experiments could be obtained by performing band structure calculations for both Ba122 and Eu122 compounds using the LDA+U approach, as detailed in Sec. II. As usually performed in these materials [13–16], in order to improve the agreement between the calculated and the measured frequencies, we have shifted the energies of the α, δ, and γ bands of Ba122 by +48, −54, and +35 meV, respectively, and those of Eu122 by +41, −54, and −30 meV, respectively. The resultant Fermi surfaces are display in Fig. 5 along with the identification of the pockets. The calculated effective masses m^*_{DFT} also display agreement with the experimental data, as shown in Table I. We note that an ideal quantitative agreement of effective masses is often

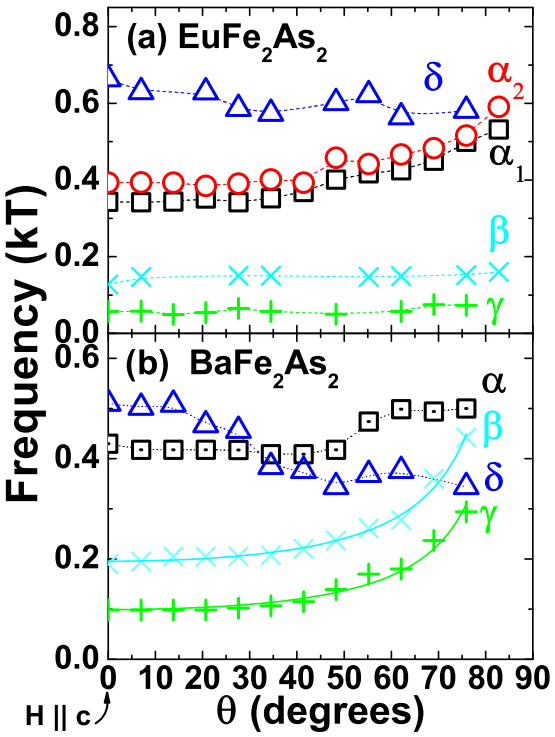

FIG. 4. (Color online) Angular field dependence (anisotropy) of the observed QO frequencies of (a) $EuFe_2As_2$ (Eu122) and (b) $BaFe_2As_2$ (Ba122).

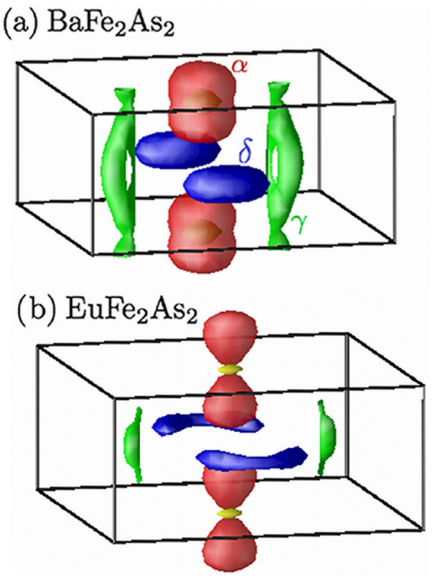

FIG. 5. (Color online) The shifted Fermi surfaces of (a) $BaFe_2As_2$ and (b) $EuFe_2As_2$ compounds in the magnetic phase. We identify the large hole sheet (red) as the α pocket, the crescent electron sheet (blue) as the δ pocket, and the tubelike electron pocket (green) as the γ pocket.

hindered by the sensitivity of the calculations to the Fermi level and to the magnetic moment.

Nevertheless, although both Fermi surfaces are very similar, a quantitative analysis of the anisotropy can be performed by using the ratio between the extremal areas at 90° and 0°. The extracted values for the anisotropy ratio $R = F(90°)/F(0°)$ are displayed in Table I. Our results show that all bands in Ba122 have higher R values than Eu122, confirming that they are more anisotropic. Remarkably, the most prominent difference in anisotropy between Ba122 and Eu122 is observed in the γ pocket, in excellent agreement with our experimental results.

Intriguingly, we also find that the Fermi surfaces in $EuFe_2As_2$ split when the calculations assume that the Eu moments ferromagnetically align with one another. The calculated splitting occurs for all three surfaces, but is significantly more prominent in the α and δ pockets. No such splitting is observed in $BaFe_2As_2$ likely due to the lack of spin moments in the intercalant plane.

In addition, it is worth mentioning that our macroscopic understanding about the underlying physics of these materials is in great agreement with the findings from an independent microscopic spin probe technique, namely, electron spin resonance (ESR). Recent reported ESR measurements also revealed an increase of both anisotropy and localization of the Fe $3d$ bands at the FeAs plane in $Eu_{1-x}Ba_xFe_2As_2$ with increasing x content [29,30]. Moreover, ESR data also pointed to a similar density of states for both under and overdoped $Ba_{1-x}Eu_xFe_2As_2$ compounds.

Enlightened by previous microscopic measurements and calculations, we suggest a plausible scenario for the role of local distortions on the fermiology of Eu122 and Ba122. Previous extended X-ray absorption fine structure (EXAFS) measurements on In-grown Ba122 single crystals revealed a decrease of the Fe-As distances as T_{SDW} is suppressed by either chemical substitution (K and Co) or applied pressure [31]. In addition, DFT+DFMT calculations also predicted a decrease of the planar xy orbital contribution to the FS as the Fe-As distance is increased [10]. Within this context, our present data combined with microscopic techniques suggest that the As ions are located further away from the Fe plane, i.e., the Fe-As tetrahedra have greater height. In fact, the height of the Fe-As tetrahedra defined as z_{As} is known to be greater in Eu122 ($z_{As} = 0.362$, [32]) than in Ba122 ($z_{As} = 0.3545(1)$, [2]). Further EXAFS measurements might provide relevant ingredients to this scenario.

In summary, we have observed Shubnikov–de Haas effect by performing high-field electrical resistivity measurements on high quality single crystals of $EuFe_2As_2$ and $BaFe_2As_2$. Although three low frequency pockets are observed for both compounds with comparable sizes and effective masses, our results show that the electronic structure in Eu122 is much more isotropic and three-dimensional when compared with Ba122, suggesting that all the Fe $3d$ orbitals contribute evenly to the FS in the Eu-rich extreme. Our main finding sheds light on the mechanism of the spin-density wave phase suppression which leads to the emergence of unconventional superconductivity in this family of materials.

ACKNOWLEDGMENTS

This work was supported by FAPESP-SP, AFOSR MURI, CNPq, and FINEP-Brazil. L.B. is supported by DOE-BES through Award No. DE-SC0002613. Work at NHMFL was performed under the auspices of the NSF through Grant No. NSF-DMR-0084173 and the State of Florida. Funding for M.D.J. was provided by the U.S. Office of Naval Research through the Naval Research Laboratory's Basic Research Program.

[1] Y. Kamihara, T. Watanabe, M. Hirano, and H. Hosono, J. Am. Chem. Soc. **130**, 3296 (2008).

[2] M. Rotter, M. Tegel, D. Johrendt, I. Schellenberg, W. Hermes, and R. Pöttgen, Phys. Rev. B **78**, 020503(R) (2008).

[3] M. Rotter, M. Tegel, and D. Johrendt, Phys. Rev. Lett. **101**, 107006 (2008).

[4] C. Wang, L. Li, S. Chi, Z. Zhu, Z. Ren, Y. Li, Y. Wang, X. Lin, Y. Luo, S. Jiang, X. Xu, G. Cao, and Z. Xu, Europhys. Lett. **83**, 67006 (2008).

[5] K. Ishida, Y. Nakai, and H. Hosono, J. Phys. Soc. Japan **78**, 062001 (2009); D. C. Johnston, Adv. Phys. **59**, 803 (2010); J. Paglione and R. L. Greene, Nat. Phys. **6**, 645 (2010); P. C. Canfield and S. L. Bud'ko, Annu. Rev. Cond. Mat. Phys. **1**, 27 (2010); H. H. Wen and S. Li, *ibid.* **2**, 121 (2011); G. R. Stewart, Rev. Mod. Phys. **83**, 1589 (2011).

[6] R. R. Urbano, E. L. Green, W. G. Moulton, A. P. Reyes, P. L. Kuhns, E. M. Bittar, C. Adriano, T. M. Garitezi, L. Bufaiçal, and P. G. Pagliuso, Phys. Rev. Lett. **105**, 107001 (2010).

[7] B. Zhou, Y. Zhang, L.-X. Yang, M. Xu, C. He, F. Chen, J.-F. Zhao, H.-W. Ou, J. Wei, B.-P. Xie, T. Wu, G. Wu, M. Arita, K. Shimada, H. Namatame, M. Taniguchi, X. H. Chen, and D. L. Feng, Phys. Rev. B **81**, 155124 (2010).

[8] S. de Jong, E. van Heumen, S. Thirupathaiah, R. Huisman, F. Massee, J. B. Goedkoop, R. Ovsyannikov, J. Fink, H. A. Drr, A. Gloskovskii, H. S. Jeevan, P. Gegenwart, A. Erb, L. Patthey, M. Shi, R. Follath, A. Varykhalov, and M. S. Golden, Europhys. Lett. **89**, 27007 (2010).

[9] H. Ding, K. Nakayama, P. Richard, S. Souma, T. Sato, T. Takahashi, M. Neupane, Y.-M. Xu, Z.-H. Pan, A. V. Federov, Z. Wang, X. Dai, Z. Fang, G. F. Chen, J. L. Luo, and N. L. Wang, J. Phys. Condens. Matt. **23**, 135701 (2011).

[10] Z. P. Hin, K. Haule, and G. Kotliar, Nat. Mater. **10**, 932 (2011).

[11] S. Thirupathaiah, Ph.D. thesis, Helmholtz-Zentrum Berlin, Albert-Einstein-Strasse, 2011.

[12] D. Schoenberg, *Magnetic Oscillations in Metals* (Cambridge University Press, Cambridge, 1984).

[13] S. E. Sebastian, in *Magnetism and Superconductivity: From Cuprates to Iron-Pnictides* (Pan Stanford, Singapore, 2012), Chap. 4.

[14] S. E. Sebastian, J. Gillett, N. Harrison, P. H. C. Lau, D. J. Singh, C. H. Mielke, and G. G. Lonzarich, J. Phys.: Cond. Matt. **20**, 422203 (2008).
[15] J. G. Analytis, R. D. McDonald, J.-H. Chu, S. C. Riggs, A. F. Bangura, C. Kucharczyk, M. Johannes, and I. R. Fisher, Phys. Rev. B **80**, 064507 (2009).
[16] T. Terashima, N. Kurita, M. Tomita, K. Kihou, C.-H. Lee, Y. Tomioka, T. Ito, A. Iyo, H. Eisaki, T. Liang, M. Nakajima, S. Ishida, S.-i. Uchida, H. Harima, and S. Uji, Phys. Rev. Lett. **107**, 176402 (2011).
[17] N. Harrison, R. D. McDonald, C. H. Mielke, E. D. Bauer, F. Ronning, and J. D. Thompson, J. Phys. Condens. Matter **21**, 322202 (2009).
[18] N. Kurita, M. Kimata, K. Kodama, A. Harada, M. Tomita, H. S. Suzuki, T. Matsumoto, K. Murata, S. Uji, and T. Terashima, J. Phys.: Conf. Ser. **273**, 012098 (2011).
[19] H. S. Jeevan, Z. Hossain, D. Kasinathan, H. Rosner, C. Geibel, and P. Gegenwart, Phys. Rev. B **78**, 052502 (2008).
[20] S. Jiang, Y. Luo, Z. Ren, Z. Zhu, C. Wang, X. Xu, Q. Tao, G. Cao and Z. Xu, New J. Phys. **11**, 025007 (2009).
[21] T. M. Garitezi, C. Adriano, P. F. S. Rosa, E. M. Bittar, L. Bufaical, R. L. de Almeida, E. Granado, T. Grant, Z. Fisk, M. A. Avila, R. A. Ribeiro, P. L. Kuhns, A. P. Reyes, R. R. Urbano, and P. G. Pagliuso, Brazilian J. Phys. **43**, 223 (2013).
[22] P. Blaha, K. Schwarz, G. K. H. Madsen, D. Kvasnick and J. Luitz, *WIEN2K* (Karlheinz Schwarz, Techn. Universitat Wien, Vienna, Austria, 2001).
[23] J. P. Perdew and Y. Wang, Phys. Rev. B **45**, 13244 (1992).
[24] V. I. Anisimov, J. Zaanen, and O. K. Andersen, Phys. Rev. B **44**, 943 (1991).
[25] Y. Xiao, Y. Su, M. Meven, R. Mittal, C. M. N. Kumar, T. Chatterji, S. Price, J. Persson, N. Kumar, S. K. Dhar, A. Thamizhavel, and Th. Brueckel, Phys. Rev. B **80**, 174424 (2009).
[26] Q. Huang, Y. Qiu, Wei Bao, M. A. Green, J. W. Lynn, Y. C. Gasparovic, T. Wu, G. Wu, and X. H. Chen, Phys. Rev. Lett. **101**, 257003 (2008).
[27] Y. Xiao *et al.*, Phys. Rev. B **81**, 220406(R) (2010).
[28] D. Graf, R. Stillwell, T. P. Murphy, J.-H. Park, E. C. Palm, P. Schlottmann, R. D. McDonald, J. G. Analytis, I. R. Fisher, and S. W. Tozer, Phys. Rev. B **85**, 134503 (2012).
[29] P. F. S. Rosa, C. Adriano, W. Iwamoto, T. M. Garitezi, T. Grant, Z. Fisk, and P. G. Pagliuso, Phys. Rev. B **86**, 165131 (2012).
[30] P. F. S. Rosa, C. Adriano, T. M. Garitezi, T. Grant, Z. Fisk, R. R. Urbano, and P. G. Pagliuso, Sci. Rep. **4**, 6543 (2014).
[31] E. Granado, L. Mendonça-Ferreira, F. Garcia, G. de M. Azevedo, G. Fabbris, E. M. Bittar, C. Adriano, T. M. Garitezi, P. F. S. Rosa, L. F. Bufaiçal, M. A. Avila, H. Terashita, and P. G. Pagliuso, Phys. Rev. B **83**, 184508 (2011).
[32] H. Raffius, E. Morsen, B. D. Mosel, W. Muller, W. Warmuth, W. Jeitschko, L. Terbuchte, and T. J. Vomhof, J. Phys. Chem. Solids **54**, 135 (1993).